A Range Deception Interference Recognition and Target Detection Method Based on Coherent Fusion Processing for Multistatic Radar System

Wei Li, Xiaolong Li*, Fan Yang, Guolong Cui and Xiaobo Yang
School of Information and Communication Engineering
University of Electronic Science and Technology of China
Chengdu, China
Email: xiaolongliuestc@gmail.com

***Abstract*—When detecting high-speed targets, the strong spoofing of range deception interference (RDI) can lead to failure of true target detection. Fortunately, the fusion processing provides an effective solution to this problem. In this paper, the target echo model under RDI conditions is established based on the range history model for multistatic radar system. On this basis, we propose an effective RDI recognition and target detection method based on coherent fusion processing. Specifically, the method firstly realizes the coherent fusion of single-channel echo by Radon Fourier transform (RFT). Then, topology-based entropy circulation matching (TECM) is used to accomplish the acquisition of the matching positions about target and RDI in different channels. Finally, the matching position is processed by elliptic positioning (EP) to realize the recognition of RDI and target. Simulation experiments verify the effectiveness of the method.**

***Index Terms*—range deception interference, high-speed target, entropy, elliptic positioning, radar target detection, coherent fusion**

I. Introduction

Moving target detection and recognition has always been a hot research topic in the field of radar signal processing, which has a broad application prospect in both civil and military fields [1], [2]. However, high-speed and stealth targets appear one after another, bringing great challenges to the accurate detection of targets [3], [4]. At the same time, digital radio frequency memory (DRFM) can generate deceptive interference signals that are highly realistic to radar signals [5]–[7], making target detection more difficult.

For deceptive interference, single-station radar can identify it by object surface scattering intensity [8], polarization characteristic difference [9], and DRFM quantization error [10]. However, the single-station radar has a single observation view and cannot obtain complete environmental information. In the face of high fidelity deception interference, it often fails to play the expected anti-interference effect.

This work was supported in part by the National Natural Science Foundation of China under Grant 62371113, in part by the Young Elite Scientists Sponsorship Program by CAST under Grant YESS20200082, in part by the Natural Science Foundation of Sichuan Province under Grant 2023NSFSC1386, and in part by the Aeronautical Science Foundation under Grant 2023Z017080001. (corresponding author: Xiaolong Li)

Therefore, multistatic radar has received widespread attention in the direction of anti-deception interference and moving target accumulation detection in recent years due to its wide perspective and flexible configuration. The different transmitting signals for different stations and joint frequency domain cooperative waveform strategy was designed in [11] to accomplish the suppression of multi-major flap blanket interference, but it is not universal. [12] invented a multistatic cooperative deception interference identification method by fusing the detection data from each radar station. However, the method is a data-level fusion with performance limitations. In [13], the authors proposed an anti-interference technique based on homologous localization for the problem of range deception interference (RDI) in multistatic radar systems. But it is not applicable to low signal-to-noise ratio (SNR) environments. [14] proposed a detection algorithm based on noncoherent fusion and designed a joint target detection and deception interference suppression method, simulation experiments proved its effectiveness. Nevertheless, the noncoherent fusion made the algorithm suffer from certain performance loss. In [15], a multi-channel coherent fusion algorithm with entropy as the optimization criterion was proposed, which improved the echo SNR. However, it did not take into account the effect of interference on the radar system in the complex electromagnetic environment.

In summary, the fusion processing is of great significance and application value for the identification of deception interference. Therefore, this paper proposes an effective RDI recognition and target detection method based on coherent fusion processing for multistatic radar system. Firstly, we establish the echo model containing the RDI. Secondly, Radon Fourier transform (RFT) is used to achieve echo coherent fusion of single-channel. Next, multi-channel signal fusion and matching location acquisition are carried out by topology-based entropy circulation matching (TECM) for target and RDI. Finally, elliptic positioning (EP) is utilized for interference and target identification. The simulation verifies that the proposed method has superior interference and target identification performance under different jamming-to-signal ratio (JSR) conditions.

II. Signal Model

A. System Description and Range History Model

This article considers a multistatic radar system, in which there exists a moving target with a jammer. Fig.1 shows the spatial scenario of this system. The position of the transmitter is $\mathbf{R}_T = (x_T, y_T)^T$. The locations of the receiving stations are $\mathbf{R}_{R1} = (x_{R1}, y_{R1})^T$, $\mathbf{R}_{R2} = (x_{R2}, y_{R2})^T$, $\cdots$, $\mathbf{R}_{RH} = (x_{RH}, y_{RH})^T$, respectively. At the same time, it is assumed that the moving target is within the radar detection power, its position is $\mathbf{R}_P = (x, y)^T$, and its velocity is $\mathbf{v} = (v_x, v_y)^T$.

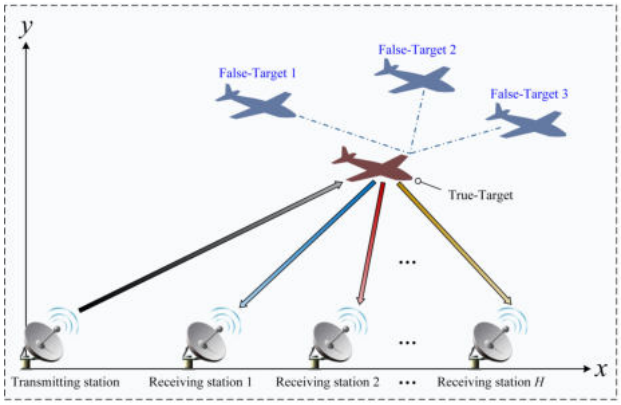

Fig. 1. Multistatic radar system space scenario.

To simplify analysis, three receiving stations radar system are selected. The echo path corresponding to transmission by the transmitting station and reception by the receiving station $k\,(k = 1, 2, 3)$ is defined here as the channel k.

The range history between the transmitter and the target $\mathbf{R}_{TP}(t_m)$, and the range history between the target and each receiver $\mathbf{R}_{PRk}(t_m)$ can be written as

$$\mathbf{R}_{TP}(t_m) = \mathbf{R}_{TP0} + \mathbf{v}t_m, \tag{1}$$

$$\mathbf{R}_{PRk}(t_m) = \mathbf{R}_{PRk0} - \mathbf{v}t_m, \tag{2}$$

where $\mathbf{R}_{TP0}$ and $\mathbf{R}_{PRk0}$ respectively denote the initial distance vectors between the transmitter and each receiver to the target, t_m is the slow time, and $m = 1, 2, \cdots, M$, M is the pulse number.

By equivalence and approximation processing, the range history of each channel in the system can be simplified as [16]

$$R_k(t_m) = R_k + V_k t_m, \tag{3}$$

where $R_k = R_{TP0} + R_{PRk0}$ and $V_k = \mathbf{R}_{TP0} \cdot \mathbf{v}/R_{TP0} - \mathbf{R}_{PRk0} \cdot \mathbf{v}/R_{PRk0}$ can be regarded as the equivalent initial distance and velocity of the target relative to the radar system channel k, respectively. And R_{TP0}, R_{PRk0} correspond to the Euclidean norms of $\mathbf{R}_{TP0}$ and $\mathbf{R}_{PRk0}$, severally.

B. Echo Model

Assuming that the transmitter transmits the linear frequency modulated signal, i.e.

$$S_t(t) = \text{rect}\,(t/T_P) \exp\left[j2\pi f_c t + j\pi\mu t^2\right], \tag{4}$$

where $\text{rect}\,(\cdot)$ is the rectangular window function, t is the fast time, T_p is the pulse width, μ is the frequency modulation slope and f_c is the signal carrier frequency.

Ignoring the noise effect, the down-conversion frequency of the target echo signal received at each receiver can be expressed as

$$\begin{aligned} S_{rk}(t, t_m) = {} & A_r S_t\left(t - R_k(t_m)/c\right) \\ & \times \exp\left[j\left(-2\pi f_c R_k(t_m)/c\right)\right], \end{aligned} \tag{5}$$

where A_r is the echo amplitude.

The down-conversion of the RDI signal received by each receiver can be expressed as [17]

$$\begin{aligned} J_{rk}(t, t_m) = {} & \sum_{i=1}^{N} A_r^J S_t\left(t - R_k(t_m)/c - \tau_i^J\right) \\ & \times \exp\left[j\left(-2\pi f_c\left(R_k(t_m)/c + \tau_i^J\right)\right)\right], \end{aligned} \tag{6}$$

where A_r^J is the interference amplitude, N is the number of false targets, and τ_i^J is the time delay of each false target.

So, the baseband echo signal received by each receiver are

$$Z_k(t, t_m) = S_{rk}(t, t_m) + J_{rk}(t, t_m). \tag{7}$$

The pulse compression (PC) process is applied to (7) and the result of PC is

$$\begin{aligned} Z_k^{pc}(t, t_m) = {} & A_e \text{sinc}\left[B\left(t - R_k(t_m)/c\right)\right] \exp\left[-j2\pi R_k(t_m)/\lambda\right] \\ & + \sum_{i=1}^{N} A_e^J \text{sinc}\left[B\left(t - R_k(t_m)/c - \tau_i^J\right)\right] \exp\left[-j2\pi R_k(t_m)/\lambda\right], \end{aligned} \tag{8}$$

where A_e is the target PC signal amplitude, A_e^J is the interference PC signal amplitude, B is the bandwidth, and λ is the wavelength.

III. The Range Deception Interference Recognition and Target Detection Method

As shown in (8), the existence of range false targets leads to the failure of the radar system to detect the true target. Therefore, this paper proposes a RDI recognition and target detection method based on coherent fusion processing, which realizes the recognition of RDI and the improvement of echo SNR in multistatic radar system. Fig.2 illustrates the flow of the proposed method.

A. RFT-Based Intra-Channel Fusion

Since it is a moving target, the RFT is needed in each channel to correct the range migration by the relative motion between the target and radar. RFT performs distance searches of range $\left[r_{\min}^k, r_{\max}^k\right]$ at intervals of $\Delta r = c/(2f_s)$ and velocity searches of range $\left[v_{\min}^k, v_{\max}^k\right]$ at intervals of Δv. Thus, the number of distance and velocity searches can be determined as $N_r^k = \text{round}\left[\left(r_{\max}^k - r_{\min}^k\right)/\Delta r\right]$ and $N_v^k = \text{round}\left[\left(v_{\max}^k - v_{\min}^k\right)/\Delta v\right]$, respectively. Where $\text{round}\,(\cdot)$ denotes the rounding operation.

Therefore, the search sequence of distance and velocity are

$$\begin{cases} r_k(l_k) = r_{\min}^k + l_k \Delta r, \ l_k = 1, \cdots, N_r^k \\ v_k(n_k) = v_{\min}^k + n_k \Delta v, \ n_k = 1, \cdots, N_v^k. \end{cases} \tag{9}$$

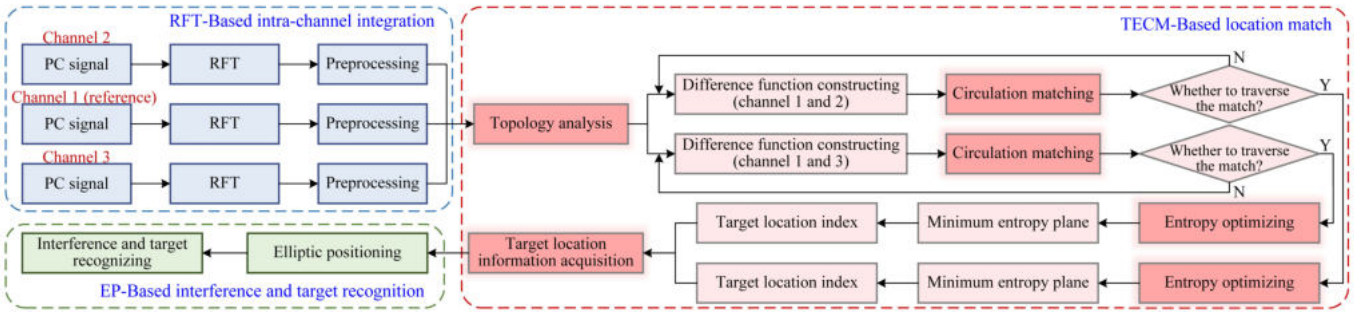

Fig. 2. Procedure of the Proposed Method.

Then the RFT coherent fusion results corresponding to PC signal of each channel in (8) are as follows

$$\begin{aligned}&\mathrm{RFT}_k\left(r_k(l_k), v_k(n_k)\right)\\&=\sum_{m=1}^{M}\left\{A_e \mathrm{sinc}\left[B\cdot f\left(r_k(l_k), v_k(n_k)\right)/c\right]\right.\\&\left.+\sum_{i=1}^{N} A_e^J \mathrm{sinc}\left[B\left(f\left(r_k(l_k), v_k(n_k)\right)-R_i^J\right)/c\right]\right\}\\&\times \exp\left[-j2\pi\left(R_k+V_k m T_r\right)/\lambda\right]\exp\left[j2\pi v_k(n_k) m T_r/\lambda\right],\end{aligned} \tag{10}$$

where $f\left(r_k(l_k), v_k(n_k)\right)=r_k(l_k)-R_k+\left(v_k(n_k)-V_k\right)mT_r$, $R_i^J=\tau_i^J\cdot c$ is the distance of individual false target and T_r is the pulse repetition time.

As shown in (10), the RFT will obtain different fusion outputs for different combinations of search parameters. When the search parameters match the equivalent parameters, the RFT fusion of the target signal will output the maximum value. Subsequently, in order to suppress the noise, we perform constant false alarm rate (CFAR) detection preprocessing on the RFT fusion output to obtain the echo after noise suppression [18]–[20]. Meanwhile, according to the preprocessing results, we can get the information of the target and RDI (namely, range and velocity) which exceeds the detection threshold. That is $\left(\hat{r}_{k1}, \hat{v}_{k1}\right), \cdots, \left(\hat{r}_{kq}, \hat{v}_{kq}\right), \cdots, \left(\hat{r}_{kN_t}, \hat{v}_{kN_t}\right)$. Where $q=1, \cdots, N_t$, and $N_t=N+1$.

B. TECM-Based Location Matching

In this section, we propose TECM to realize the acquisition of distance and velocity for target and RDI in each channels.

1) Topology Analysis: For subsequent derivation, the N_t target estimation parameters in each channel, in ascending order of distance, are $\left(\hat{r}_{k1}^r, \hat{v}_{k1}^r\right)$, $\cdots$, $\left(\hat{r}_{kq}^r, \hat{v}_{kq}^r\right)$, $\cdots$, $\left(\hat{r}_{kN_t}^r, \hat{v}_{kN_t}^r\right)$. Without loss of generality, we assume that the u-th target in each channel is the true target, and the difference in distance between each of the remaining targets and true target can be determined as

$$\hat{r}_{ku}^r-\hat{r}_{kq}^r=R_{uq}^k, \tag{11}$$

where R_{uq}^k represents the distance difference between the q-th target in the k-th channel and the true target.

From (10), the peak position of the true target differs from each RDI by a fixed time delay shift. Therefore, in the $R-V$ fusion detection plane of each channel, the targets have the same spatial topology. Therefore, we can obtain

$$R_{uq}=R_{uq}^1=R_{uq}^2=R_{uq}^3, \tag{12}$$

where R_{uq} represents the distance difference between the q-th target and the true target of any channel.

2) Circulation Matching: We assume that the number of targets after preprocessing in each channel is: C_1, C_2 and C_3, respectively. Where $C_i \geq N_t, i=1,2,3$. Correspondingly, we define the parameter estimation results for the targets in each channel as $\left(\hat{r}_{k1}^c, \hat{v}_{k1}^c\right), \cdots, \left(\hat{r}_{km_k}^c, \hat{v}_{km_k}^c\right), \cdots, \left(\hat{r}_{kC_k}^c, \hat{v}_{kC_k}^c\right)$. Where $m_k=1,2,\cdots,C_k$.

For ease of analysis, we select the first target of channel 1 as the reference target. Then, each target in other channels is looped to do the matching process with that reference target. Let's take channel 2 as an example, the relative range differences between each target and reference target could be denoted as

$$\mathbf{H}^r\left(\hat{r}_{11}^c, \hat{r}_{2m_2}^c\right)=\left[\hat{r}_{11}^c-\hat{r}_{21}^c, \cdots, \hat{r}_{11}^c-\hat{r}_{2C_2}^c\right]^{\mathrm{T}}. \tag{13}$$

Similarly, the relative velocity differences between each target and reference target can be expressed as

$$\mathbf{H}^v\left(\hat{v}_{11}^c, \hat{v}_{2m_2}^c\right)=\left[\hat{v}_{11}^c-\hat{v}_{21}^c, \cdots, \hat{v}_{11}^c-\hat{v}_{2C_2}^c\right]^{\mathrm{T}}. \tag{14}$$

Here, we define $\mathbf{H}_l^r$ to be the l-th element of $\mathbf{H}^r\left(\hat{r}_{11}^c, \hat{r}_{2m_2}^c\right)$ and $\mathbf{H}_l^v$ to be the l-th element of $\mathbf{H}^v\left(\hat{v}_{11}^c, \hat{v}_{2m_2}^c\right)$. Thus, utilizing (13) and (14), the corresponding envelope alignment function between each target in channel 2 and reference target can be constructed as

$$H_l^e\left(r_2(l_2), v_2(n_2)\right)=\delta\left(r_2(l_2)-\mathbf{H}_l^r\right)\delta\left(v_2(n_2)-\mathbf{H}_l^v\right), \tag{15}$$

where $l=1,2,\cdots,C_2$ and $\delta(\cdot)$ denotes the Dirichlet function.

In addition, according to (10), the phase compensation function between each target in channel 2 and reference target can be written as

$$\mathbf{H}^p\left(\hat{r}_{11}^c, \hat{r}_{2m_2}^c\right)=\begin{bmatrix}\exp\left(j2\pi\left(\hat{r}_{11}^c-\hat{r}_{21}^c\right)/\lambda\right)\\ \cdots\\ \exp\left(j2\pi\left(\hat{r}_{11}^c-\hat{r}_{2C_2}^c\right)/\lambda\right)\end{bmatrix}. \tag{16}$$

Similarly, we define $\mathbf{H}_l^p$ is the l-th element of $\mathbf{H}^p\left(\hat{r}_{11}^c, \hat{r}_{2m_2}^c\right)$. Utilizing (15) and (16), the result of circulation matching about the reference target in channel 1 with each target in channel 2 can be expressed as

$$\begin{aligned}&\Upsilon_l\left(\hat{r}_{11}^c, \hat{r}_{2l}^c, \hat{v}_{11}^c, \hat{v}_{2l}^c; r_1(l_1), v_1(n_1), r_2(l_2), v_2(n_2)\right)\\&= \mathrm{RFT}_1\left(r_1(l_1), v_1(n_1)\right) + \mathrm{RFT}_2\left(r_2(l_2), v_2(n_2)\right)\mathbf{H}_l^p H_l^e.\end{aligned} \tag{17}$$

3) Entropy Optimizing: Inspired by the image phase adjustment in inverse synthetic aperture radar (ISAR) [21], this section utilizes the entropy function property of the circulation matching plane to filter system target index, i.e.

$$E_l = \sum_{m=1}^{N_r^1}\sum_{n=1}^{N_v^1}\frac{\left|g_l(m,n)\right|^2}{S_l}\ln\frac{S_l}{\left|g_l(m,n)\right|^2}, \tag{18}$$

where $g_l(m,n) = \Upsilon_l$ denotes the data of the l-th matching plane and $S_l = \sum_{m=1}^{N_r^1}\sum_{n=1}^{N_v^1}\left|g_l(m,n)\right|^2$.

In the C_2 circulation matching planes corresponding to (17), correct match corresponds to a lower entropy value because all system targets have obtained coherent fusion gain. Here we select the matching result with the lowest entropy as the correct match of the reference target, i.e. $E_1 = \min E_{m_2}$. The correctly matched target index can be written as $l_1 = \arg\min_{m_2} E_{m_2}$. By repeating the circulation matching process with each target in channel 1 as the reference target, the C_1 optimal matches can be obtained. As a result, the corresponding target index in channel 2 can be denoted as $l_1, l_2, \cdots, l_{C_1}$ and the entropy can be denoted as $E_1, E_2, \cdots, E_{C_1}$.

When any system target is chosen as the reference target, the optimal match will be the same matching plane. In other words, it has the same and minimum entropy value. Therefore, the system target index can be expressed as

$$[\mathbf{I}, \mathbf{K}_I] = \underset{m_1, l_{m_1}}{\arg}\left(\min(E_{m_1})\right), \tag{19}$$

where $\mathbf{I} = [H_1, \cdots, H_{N_t}]$ and $\mathbf{K}_I = [K_{H_1}^I, \cdots, K_{H_{N_t}}^I]$ represent the system target indexes for channel 1 and channel 2, respectively.

Similarly, repeating (13) - (19), the optimal matching result with channel 1 as the reference channel and channel 3 can be obtained, and the system target index is $[\mathbf{Q}, \mathbf{K}_Q]$.

4) Target Location Information Acquisition: The circulation matching all take channel 1 as the reference channel, so the system target index arrays $\mathbf{I}$ and $\mathbf{Q}$ of channel 1 have the same set of elements in the optimal match. Therefore, we obtain the element mapping relationship between the system target index arrays $\mathbf{K}_I$ and $\mathbf{K}_Q$ of channel 2 and 3. The specific results are as Table I.

Table I shows the parameter indexes of the system targets, which can be combined with the estimated location of preprocessing to obtain the $R-V$ estimation information of all targets in different channels. But how to distinguish the true target and RDI from these targets requires elaboration.

TABLE I
SYSTEM TARGET INDEX.

	Target 1	**Target 2**	$\cdots$	**Target q**	$\cdots$	**Target** N_t
Channel 1	H_1	H_2	$\cdots$	H_q	$\cdots$	H_{N_t}
Channel 2	$K_{H_1}^I$	$K_{H_2}^I$	$\cdots$	$K_{H_q}^I$	$\cdots$	$K_{H_{N_t}}^I$
Channel 3	$K_{H_1}^Q$	$K_{H_2}^Q$	$\cdots$	$K_{H_q}^Q$	$\cdots$	$K_{H_{N_t}}^Q$

C. EP-Based Interference and Target Recognition

In this section, we use EP in conjunction with N_t target transmission paths, and radar system topology relationships to achieve authentic recognition of target and RDI. Fig.3 illustrates the EP schematic for the multistatic radar system.

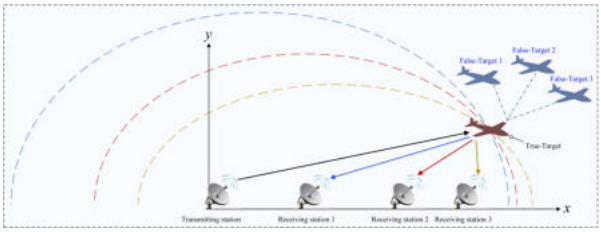

Fig. 3. Multistatic radar system EP schematic.

As in Fig.3, with reference to the true target, we take the location of transmitter and receiver station 1 as the focus, the estimated value of the equivalent distance as the semi-major axis, the blue ellipse can be constructed. Similarly, ellipses with true targets in other channels are constructed, namely the red and yellow ellipses in Fig.3.

Taking an arbitrary target q as an example, we construct elliptic equations

$$\begin{cases}\left(x - x_{R1}/2\right)^2/{a_1}^2 + y^2/{b_1}^2 = 1\\ \left(x - x_{R2}/2\right)^2/{a_2}^2 + y^2/{b_2}^2 = 1\\ \left(x - x_{R3}/2\right)^2/{a_3}^2 + y^2/{b_3}^2 = 1,\end{cases} \tag{20}$$

where the semi-major axis $a_k = \hat{r}_{kq}/2$ of the ellipse is half of the equivalent distance of target q in channel k, and the focal length $2c_k = x_{Rk}$ of the ellipse is the distance between the transmitting station and receiving station in channel k.

Using mathematical methods to solve equation 1 and 2 in (20) by association [22], the coordinates of the intersection position of the corresponding ellipse can be obtained as

$$x_{12} = -{a_1}^2{b_2}^2\left(x_{R1} - x_{R2}\right)/\left(2{a_1}^2{b_2}^2 - 2{a_2}^2{b_1}^2\right) + x_{R1}/2, \tag{21}$$

$$y_{12} = b_1\sqrt{1 - \left[a_1 b_2^2\left(x_{R1} - x_{R2}\right)/\left(2{a_1}^2{b_2}^2 - 2{a_2}^2{b_1}^2\right)\right]^2}. \tag{22}$$

Similarly, solving the remaining combinations of equations in (20) can obtain x_{13}, y_{13}, x_{23} and y_{23}. Substituting the system parameters above, if the target q is the true target, we can get $x_{12} = x_{13} = x_{23}$, $y_{12} = y_{13} = y_{23}$. If the target q is the false target, then $x_{12} \neq x_{13} \neq x_{23}$, $y_{12} \neq y_{13} \neq y_{23}$

can be obtained. That is, the true target must be located on the circumference of each ellipse, while the same false target does not satisfy this result. In summary, the accurate identification of RDI is accomplished by EP for localization solving in the first quadrant.

IV. Simulation Analysis

In this section, we verify the effectiveness of the proposed method through simulation experiments. First, the radar system parameters are shown in Table II. Set the position of the target as $(45000, 16000)$ m, the velocity as $(145.2, 27.2)$ m/s. And the transmitter is located at the origin, the receiver positions are $(7990.2, 0)$ m, $(30002.3, 0)$ m and $(40026.4, 0)$ m. In addition, the JSR is 6 dB and the echo SNR after PC is -12 dB. The number of range false targets is three, and the delay modulation is done at distances of -9000 m, 15000 m and 21000 m, respectively. By calculation, the equivalent velocities of the target in each channel are 289.99 m/s, 265.07 m/s and 215.01 m/s, the equivalent distances are shown in Table III.

TABLE II
Radar System Parameters.

Parameters	Symbols	Values
Carrier frequency	f_c	0.15 GHz
Bandwidth	B	5 MHz
Pulse repetition frequency	PRF	500 Hz
Sampling frequency	f_s	10 MHz
Pulse number	M	300
Pulse duration	T_r	20 us

TABLE III
The Set and Estimated Position of Interference and Target.

	Value	Channel 1	Channel 2	Channel 3
Interference 1	Set	109080.10 m	90689.95 m	85515.01 m
	Estimated	109080 m	90690 m	85515 m
Interference 2	Set	103080.10 m	84689.95 m	79515.01 m
	Estimated	103080 m	84690 m	79515 m
Interference 3	Set	79080.10 m	60689.95 m	55515.01 m
	Estimated	79080 m	60690 m	55515 m
Target	Set	88080.10 m	69689.95 m	64515.01 m
	Estimated	88080 m	69690 m	64515 m

As shown in the PC results of Fig.4(a)-(c), the signals in all three channels are drowned in noise. After RFT coherent fusion processing in Fig.5(a)-(c), the target and interferences in each channel form visible peaks in the accumulation parameter space. In addition, the estimated values of the equivalent parameters for target and interferences can be obtained based on the preprocessing results shown in Fig.5(d)-(f). It is highly consistent with the theoretical values in Table III.

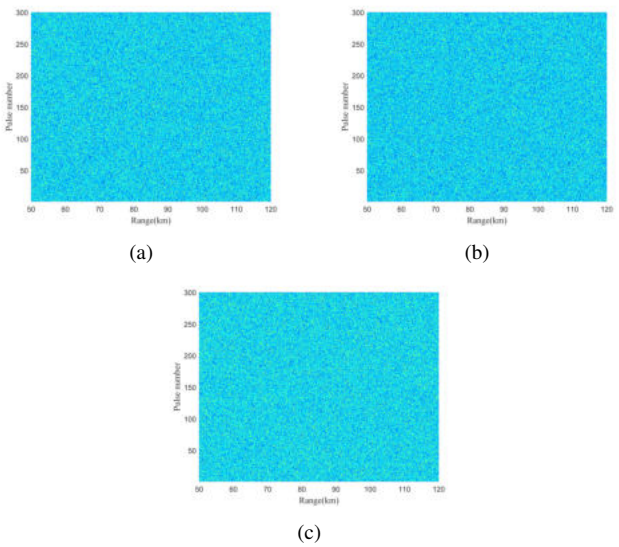

(a) (b) (c)

Fig. 4. The PC results. (a) Channel 1. (b) Channel 2. (c) Channel 3.

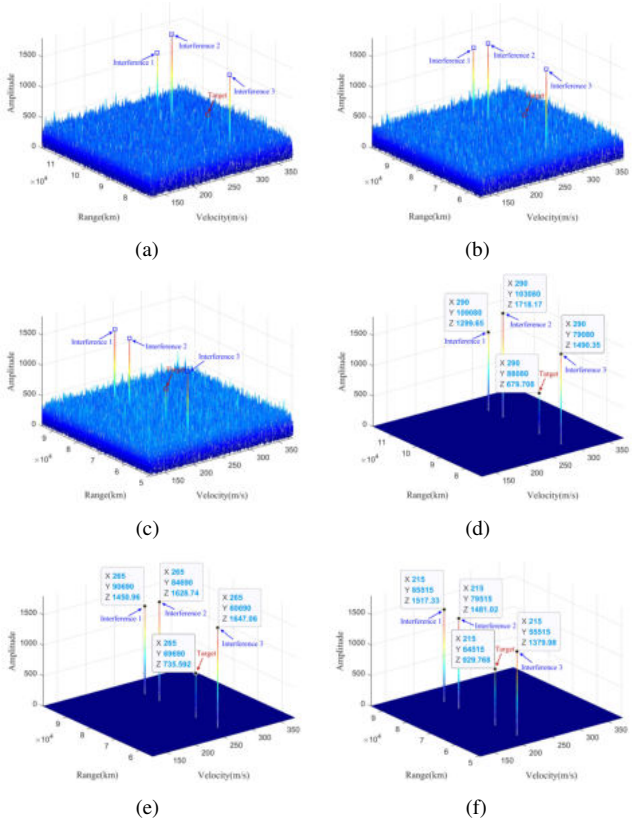

(a) (b) (c) (d) (e) (f)

Fig. 5. RFT coherent fusion and preprocessing results of each channel echoes. (a) RFT of channel 1. (b) RFT of channel 2. (c) RFT of channel 3. (d) Preprocessing of channel 1. (e) Preprocessing of channel 2. (f) Preprocessing of channel 3.

Fig.6(a) and (b) exhibit the results of correct and incorrect circulation matching between channel 1 and 2. In the case of correct match, the peak value of the system target is about twice that of the single channel. Fig.7 demonstrates the results of entropy optimization. Where there are four

minimum entropy values in each entropy plane, corresponding to the dark rectangles in Fig7.(a) and (b). Meanwhile, the coordinates where the minimum entropy values are located mean the position indexes of the system targets. In addition, the data show that the optimal match has a significant entropy difference compared to other matching cases.

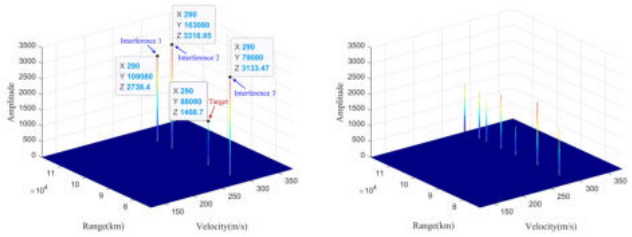

(a) (b)

Fig. 6. Circulation Matching Results. (a) Correct result. (b) Incorrect result.

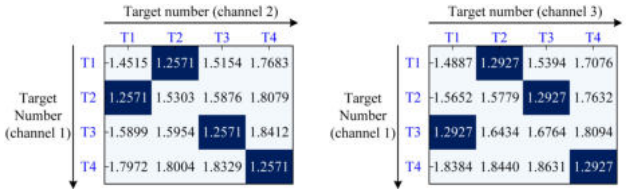

(a) (b)

Fig. 7. Optimization results after entropy. (a) Between channel 1 and 2. (b) Between channel 1 and 3.

Next, EP processing is performed on the estimated target and interference position, and the results are shown in Fig.8. The EP results of different targets have different geometrical structures. Fig.8(a), (b) and (c) all produce three two-by-two intersections and are not focused on the first quadrant, so they are EP results of RDI. At this point, Fig.8(d) produces only a unique intersection in the first quadrant, so it is judged to be the EP results of the true target.

Finally, the detection performance of the proposed method is comparatively analyzed by Monte Carlo experiments with different JSR. The result is shown in Fig.9, with a false alarm rate of $P_f = 10^{-3}$. From Fig.9, it can be seen that:

- Under the same JSR, the target detection probability rises with the increase of the SNR.
- Under the same SNR, the target detection probability gradually increases with the growth of the JSR. However, when the JSR exceeds 2 dB, the target detection probability is close to saturation and no longer grows significantly.

V. Conclusion

Aiming at the problem of high-speed target detection for multistatic radar system under RDI environment, we proposed a RDI recognition and target detection method based on coherent fusion processing. Firstly, the target echo model with interference was established. Then, RFT was used to realize the single-channel echo coherent fusion. Next, we

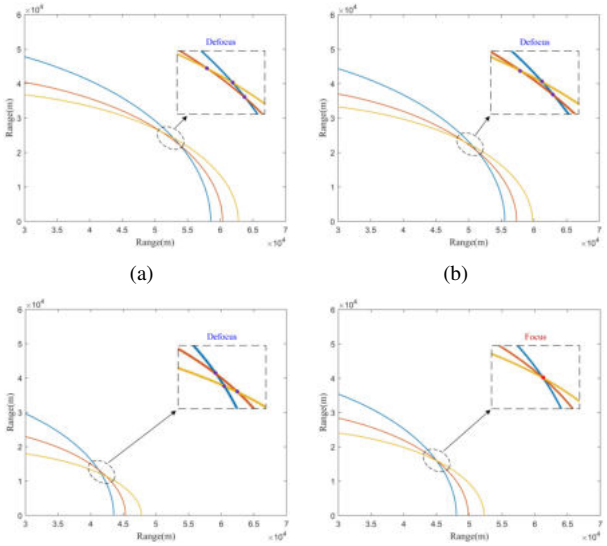

(a) (b) (c) (d)

Fig. 8. Ellipse positioning results. (a) Interference 1. (b) Interference 2. (c) Interference 3. (d)True target.

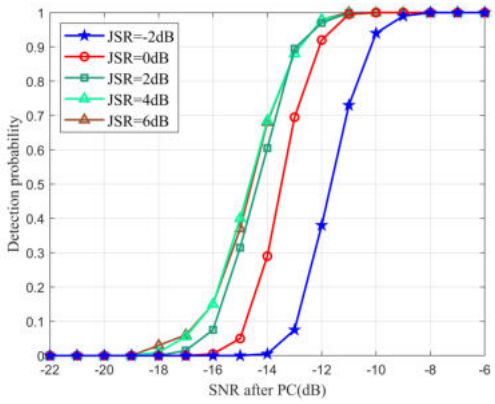

Fig. 9. Detection performance comparison.

used TECM for circulation matching, and obtained the target and RDI matching location based on entropy optimization criterion. Subsequently, the identification of RDI and target were accomplished by EP. Finally, from the digital simulation results, it can be seen that the proposed method can effectively fulfill the identification of RDI and target under the variation of interference amplitude, while realizing the fusion and enhancement of the target signal.

References

[1] M. Üney, P. Horridge, B. Mulgrew and S. Maskell, "Coherent Long-Time Integration and Bayesian Detection With Bernoulli Track-Before-Detect," *IEEE Signal Process. Lett.*, vol. 30, pp. 239-243, Mar. 2023.

[2] X. Li, Y. Yang, Z. Sun, G. Cui and T. S. Yeo, "Multi-Frame Integration Method for Radar Detection of Weak Moving Target," *IEEE Trans. Veh. Technol.*, vol. 70, no. 4, pp. 3609-3624, Apr. 2021.

[3] M. Zhan et al., "A Modified Keystone Transform Matched Filtering Method for Space-Moving Target Detection," *IEEE Trans. Geosci. Remote Sens.*, vol. 60, pp. 1-16, Sept. 2022.

[4] Z. Ding, S. Liu, Y. Li, P. You and X. Zhou, "Parametric Translational Compensation for ISAR Imaging Based on Cascaded Subaperture Integration With Application to Asteroid Imaging," *IEEE Trans. Geosci. Remote Sens.*, vol. 60, pp. 1-17, Dec. 2022.

[5] B. Rao, Z. Gu and Y. Nie," Deception Approach to Track-to-Track Radar Fusion Using Noncoherent Dual-Source Jamming," *IEEE Access*, vol. 8, pp. 50843-50858, Mar. 2020.

[6] X. Yu, W. Wang, H. Wu, J. Bo, J. Zhang and J. Meng, "Multi-Domain Feature Fusion Based Radar Deception Jamming Recognition Method," in *Proc. IEEE Int. Symp. Electromagn. Compat.*, Hangzhou, China, 2023, pp. 1-4.

[7] M. Greco, F. Gini and A. Farina, "Radar Detection and Classification of Jamming Signals Belonging to a Cone Class," *IEEE Trans. Signal Process.*, vol. 56, no. 5, pp. 1984-1993, May. 2008.

[8] J. Liu, L. Zhang, S. Zhao, N. Liu and J. Zhang, "Correlation Characteristic Analysis in Diversity Multiple-Input Multiple-Output Radar," *Electron. Lett.*, vol. 53, no. 5, pp. 349-351, Mar. 2017.

[9] Z. Zhang, J. Xie, C. Sheng and Z. Tang, "Deceptive Jamming Discrimination Based on Range-Angle Localization of a Frequency Diverse Array," *Front. Inform. Technol. Elect. Eng.*, vol. 18, pp. 1437-1446, Oct. 2017.

[10] B. Rao, S. Xiao and X. Wang, "Joint Tracking and Discrimination of Exoatmospheric Active Decoys Using Nine-Dimensional Parameter-Augmented EKF," *Signal Process.*, vol. 91, no. 10, pp. 2247-2258, Oct. 2011.

[11] R. Tan, M. Liao, Y. Bu, X. Yu and G. Cui, "Cooperative Waveforms Design for Distributed Radars in Multiple Blanket Jamming," in *Proc. IEEE Radar Conf.*, San Antonio, TX, USA, 2023, pp. 1-6.

[12] R. Song, D. Cheng, W. Qi, L. Xiang and Y. Jiang, "Research on Anti-Deceptive Jamming of Multi Station Fusion of Netted Radar," in *Proc. IEEE Jt. Int. Inf. Technol. Artif. Intell. Conf.*, Chongqing, China, 2022, pp. 1732-1734.

[13] D. Huang, G. Cui, M. Ge, X. Yu and L. Kong, "A Suppression Method Against Range Deception Jamming Based on Homologous Localisation Test," *J. Eng.*, vol. 2019, no. 20, pp. 6961-6965, Aug. 2019.

[14] S. Zhang, Y. Zhou, L. Zhang, Q. Zhang and L. Du, "Target Detection for Multistatic Radar in the Presence of Deception Jamming," *IEEE Sens. J.*, vol. 21, no. 6, pp. 8130-8141, Mar. 2021.

[15] M. Wang, X. Li, T. Fan, Z. Sun, C. Wang and G. Cui, "Entropy-Based Coherent Integration Method for Moving Target Detection Using Phased-MIMO Radar," in *Proc. IEEE Radar Conf.*, Atlanta, GA, USA, 2021, pp. 1-6.

[16] M. Wang, X. Li, L. Gao, Z. Sun, G. Cui and T. S. Yeo, "Signal Accumulation Method for High-Speed Maneuvering Target Detection Using Airborne Coherent MIMO Radar," *IEEE Trans. Signal Process.*, vol. 71, pp. 2336-2351, Jun. 2023.

[17] X. Duan, Z. He, H. Liu and J. Li, "Algorithm of Range Deception Jamming Recognition for Bistatic MIMO Radar," in *Proc. Int Conf Signal Process.*, Chengdu, China, 2016, pp. 1519-1523.

[18] W. Lei, Q. Tan, F. Hou, Z. Yang, G. Liu and Q. Gu, "A Signal Denoising Method of Gesture Radar Based on Weighted Principal Component Analysis and Improved Wavelet Threshold," in *Proc. IEEE Inf. Technol. Mechatronics Eng. Conf., ITOEC*, Chongqing, China, 2018, pp. 1675-1679.

[19] J. -H. Lee, H. -J. Moon and S. -H. Jeong, "Numerically Efficient Determination of the Optimal Threshold in Natural Frequency-Based Radar Target Recognition," *IEEE Trans. Antennas Propag.*, vol. 62, no. 11, pp. 5889-5894, Nov. 2014.

[20] R. S. Raghavan, "Analysis of CA-CFAR processors for linear-law detection," *IEEE Trans. Aerosp. Electron. Syst.*, vol. 28, no. 3, pp. 661-665, Jul. 1992.

[21] D. Ustun and A. Toktas, "Translational Motion Compensation for ISAR Images Through a Multicriteria Decision Using Surrogate-Based Optimization," *IEEE Trans. Geosci. Remote Sens.*, vol. 58, no. 6, pp. 4365-4374, Jun. 2020.

[22] L. Rui and K. C. Ho, "Elliptic Localization: Performance Study and Optimum Receiver Placement," *IEEE Trans. Signal Process.*, vol. 62, no. 18, pp. 4673-4688, Sept. 2014.